AIAA SciTech
4-8 January 2016, San Diego, California, USA
AIAA Modeling and Simulation Technologies Conference

Extending the SPeAD-M86 Model: Incorporating the Effects of $F_{10.7}$ Variations on Atmospheric Density

Siddharth S. Kedare* and Steve Ulrich†
Carleton University, Ottawa, Ontario K1S 5B6, Canada

This paper presents an extension to the SPeAD-M86 model by Kedare & Ulrich (2015) by incorporating variations in atmospheric density resulting from the 11-year solar cycle, as quantified using the $F_{10.7}$ index. It focuses on utilizing sinusoidal and exponential piece-wise functions to estimate temporal density changes in the atmosphere at geometric altitudes ranging from 0 – 1000 km. The model is validated against data from existing analytical and empirical atmospheric models. It is then implemented in a Matlab-Simulink orbit and attitude propagation environment to assess its stability, validity, and computational footprint at various instances in the solar cycle. The orbital elements from each simulation were compared against those obtained from baseline "truth" simulations run using the Naval Research Lab (NRL) MSISE-00 model. Results indicate improvements in accuracy compared to the SPeAD-M86 model with minimal increase in computational run time.

I. Introduction

CubeSats often operate at altitudes between 200 km and 1000 km within the thermosphere and exosphere regions of Earth's atmosphere, where the solar cycle can result in large density variations. At these altitudes, atmospheric drag can significantly affect spacecraft dynamics. Acting opposite to the velocity vector, atmospheric drag removes energy from an orbit, reducing the semi-major axis and the eccentricity,[1] leading to the eventual reentry of the spacecraft. The acceleration due to drag is given by

$$\ddot{\vec{r}}_{drag} = -\frac{1}{2} C_D \frac{A}{m} \rho |\vec{v_r}| \vec{v_r} \tag{1a}$$

where

$$A = \sum_{i=1}^{n} A_n \begin{cases} A_n = 0, & \text{if } \vec{A}_n \cdot \vec{v_r} < 0. \\ A_n = \vec{A}_n \cdot \vec{v_r} & \text{otherwise.} \end{cases} \tag{1b}$$

where m is the spacecraft mass, C_D is the drag coefficient, A is the total projected area perpendicular to $\vec{v_r}$, $\vec{A}_n$ is the area vector for the n^{th} spacecraft panel in the body frame, ρ is the atmospheric density, and $\vec{v_r}$ is the velocity of the spacecraft relative to the atmosphere. Similarly, the torque acting on a spacecraft due to atmospheric drag can be expressed as

$$\vec{T}_{drag} = \sum_{i=1}^{n} \vec{F}_{drag_i} \times \vec{r}_{cp_i} \tag{2}$$

where $\vec{F}_{drag_i}$ is the drag force acting on each spacecraft panel, and $\vec{r}_{cp_i}$ is the center of pressure location of each spacecraft panel in the body frame. At altitudes above 300 km, ρ can vary by orders of magnitude due to solar cycle variations. Walterscheid[2] indicates that effects of the solar cycle on atmospheric density are far more significant than the associated changes in atmospheric velocity (high-atmospheric winds) or drag coefficient. Estimation of atmospheric density is therefore essential for orbit prediction. However, minimizing computational storage and processing requirements while maintaining reasonable accuracy is

*Research Affiliate, Department of Mechanical and Aerospace Engineering, 1125 Colonel By Drive. Member AIAA.
†Assistant Professor, Department of Mechanical and Aerospace Engineering, 1125 Colonel By Drive. Senior Member AIAA.

equally critical for CubeSat applications. Existing atmospheric density models such as USSA 1976,[3] Jacchia-Bowman,[4] Jacchia 1971,[5] and NRLMSISE-00[6] which have been used previously for ground-based precision orbit determination require large lookup tables, numerical integration, or multiple inputs in addition to spacecraft position.

The SPeAD-M86 model was developed in 2015 by Kedare and Ulrich[7] as part of research towards the formulation of a torque-optimal guidance algorithm for CubeSats. This model focused on being computationally lightweight, while providing reasonably accurate atmospheric density predictions at geometric altitudes ranging from 0 to 1000 km. At the time, the model was calibrated using MSIS-86 density data based on mean $F_{10.7}$ solar activity. While sufficient to provide a mean density estimate, the authors noted that it could not account for the significant effects of the solar cycle on density variations in the upper atmosphere. The research presented herein attempts to address this limitation.

With CubeSats rapidly growing in popularity, the scientific and research communities stand to benefit from further expanding the capabilities of low-cost nanosatellites. Incorporating the ability for a spacecraft to predict atmospheric density based on spatial as well as temporal coordinates could allow for the design of long duration CubeSat missions. Applications would include the ability for CubeSats to execute on-board orbit prediction routines for long-duration missions or long-term hibernation within satellite constellations. Further uses could include the ability for CubeSats situated within the thermosphere to enter passive observation mode near the end of life and autonomously "smart de-orbit" by deploying drag sails at or near solar maximum.

This paper focuses on incorporating density variations due to solar activity as an extension to the SPeAD-M86 model named SPeAD-M86 FX ($\underline{F}_{10.7}$ e$\underline{X}$tended). The document is organized as follows: Section II provides an overview of the effects of the solar cycle on atmospheric density. Section III presents the formulation and implementation of the SPeAD-M86 FX model. Section IV details the validation routines for determining the accuracy, stability, and performance of the SPeAD-M86 FX model. In Section V, results from the validation routines are presented.

II. Effect of the Solar Cycle on Earth's Atmosphere

In response to changes in the amount of solar radiation absorbed by the thermosphere, significant variations in atmospheric temperature, density, and chemical composition are observed. The improved SPeAD-M86, hereon referred to as SPeAD-M86 FX model, developed within this paper shall focus on the effects of the $F_{10.7}$ solar cycle on atmospheric density.

II.A. Atmospheric Density

As previously discussed in Sec. I, atmospheric density, ρ, is a significant factor in calculating the atmospheric drag acting upon a satellite in Low Earth Orbit (LEO). Solar cycle variations in total density are driven primarily by the heating of the global thermosphere by solar extreme ultraviolet (EUV) radiation, with greater EUV levels increasing density. During a period of high solar activity, the Sun adds extra energy to the atmosphere, causing the atmosphere to rise and expand. The low density layers of air at LEO altitudes rise and are replaced by higher density layers that were previously at lower altitudes. As a result, the density at a specific altitude increases, and a spacecraft will experience a stronger drag force.[8] Walterscheid provides further insight into the mechanisms of density change due to EUV variations over the solar cycle by focusing on density as function of the local and integrated values of temperature and composition at a given altitude.[2] Around the solar minimum, satellites in LEO boost their orbits about four times per year in order to compensate for atmospheric drag. When solar activity is at its maximum, satellites may be required to execute maneuvers every 2-3 weeks to maintain their orbit.[8] It is therefore evident that density fluctuations due to the solar cycle can have a significant influence on spacecraft orbit.

II.B. Chemical Composition

In addition to density variations, the solar cycle variations significantly modify the chemistry of the upper atmosphere. The concentration of highly reactive species, predominantly atomic oxygen, can vary by several orders of magnitude between solar maximum and minimum depending on altitude. Atomic oxygen is a concern for spacecraft component degradation as it can react with thin organic films (primarily lubricants), advanced composites, and metallic surfaces.[9]

III. Expanding the SPeAD-M86 Model

Incorporating the 11-year solar cycle into the SPeAD-M86 model as an analytical function provides a simple and mathematically elegant solution to estimating atmospheric density while accounting for fluctuations in solar activity. Having established a piece-wise exponential relation between altitude and density, an analytical function relating atmospheric density variations to time was desired. Given the cyclic nature of the solar cycle, a sinusoidal correlation linking density and time since solar minimum was proposed.

III.A. Overview

Figure 1 illustrates the data flow between the various modules of the SPeAD-M86 FX model.

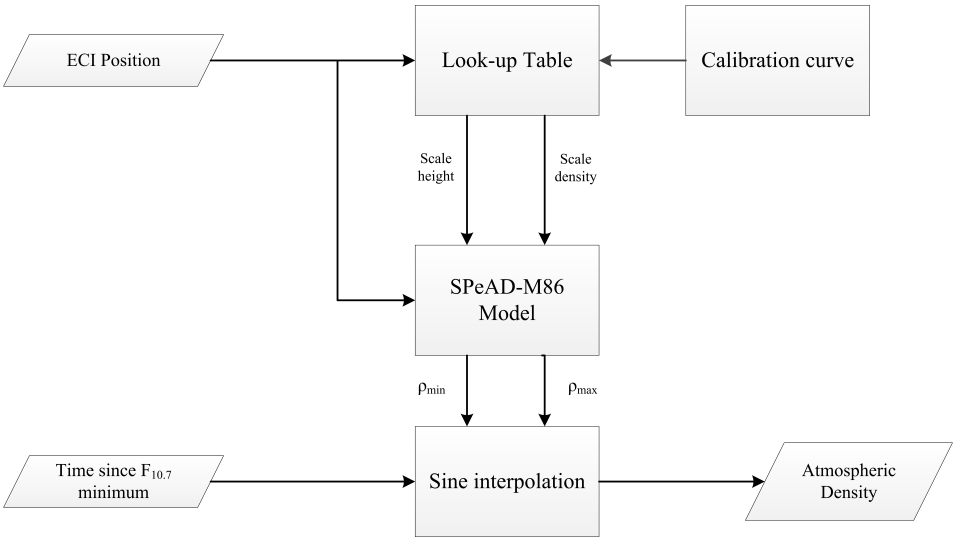

Figure 1. Extended SPeAD-M86 Model Overview

Given the position of a spacecraft in Earth Centered Inertial (ECI) coordinates, and a time since solar minimum, the SPeAD-M86 FX model calculates atmospheric density. Using a calibration curve, the scale height coefficient and scale density are calculated. These parameters are utilized by the original SPeAD-M86 model to calculate the maximum and minimum density at the specified altitude. The sine interpolation then computes a density based on the time since solar minimum. Details regarding the mathematical aspects of the individual modules are provided in Sec. III.B and Sec. III.C.

III.B. Formulation

The solar cycle can be approximated as a sinusoidal variation with a period of approximately 11 years.[10] The $F_{10.7}$ index provides a temporally stable, continuous, and well-calibrated indication of solar activity.[11] A corresponding sinusoidal variation in atmospheric density is observed for the period 1967-2010 as presented by Emmert, Lean, and Picone,[12] indicating a clear link between solar activity and atmospheric density. Furthermore, the $F_{10.7}$ index has proven empirically to be a reliable, well-calibrated indicator of thermospheric density variations,[12] as it correlates directly to the EUV flux outlined earlier in Sec. II.A.

Neglecting the effects of any time lag between the solar cycle and the resulting atmospheric density fluctuations, a sinusoidal correlation relating density at any altitude to the time since solar minimum is desired. The general form of a time-varying sine wave equation is given by

$$Y(t) = A\sin(\omega t - \phi) + B \tag{3}$$

where A is the wave amplitude, ω is the solar cycle frequency, ϕ is positive phase shift, t is the time since solar minimum in years, and B is the wave displacement. Setting $Y = \rho$, and with the knowledge that the wave amplitude is the mean of the maximum and minimum density at any altitude,

$$\rho(t) = \frac{\rho_{max} - \rho_{min}}{2}\sin(\omega t - \phi) + B \tag{4}$$

Based on the definition of t, we desire $\rho(0) = \rho_{min}$, which translates to shifting the wave horizontally by a quarter cycle to the right, or $\pi/2$, along the time axis. Expressing ω in terms of the solar cycle period T, we obtain

$$\rho(t) = \frac{\rho_{max} - \rho_{min}}{2} \sin(\frac{2\pi}{T}t - \frac{\pi}{2}) + B \tag{5}$$

Since $\rho = \rho_{min}$ at $t = 0$,we can find B and obtain

$$\rho(t) = \frac{\rho_{max} - \rho_{min}}{2} \sin(\frac{2\pi}{T}t - \frac{\pi}{2}) + \frac{\rho_{max} + \rho_{min}}{2} \tag{6}$$

The values ρ_{max} and ρ_{min} are functions of the geometric altitude, z, and are obtained using the piece-wise approach of the original SPeAD-M86 model. For completeness, this piece-wise exponential relation is now presented.

$$\rho(z) = \rho_{s_i} \exp\left(\frac{-z}{H_i}\right) \quad @ \quad h_i < z < h_{(i+1)} \tag{7}$$

where ρ_s is the scale density for a given altitude interval, z is the geometric altitude above sea level, and H_i is comparable to the scale height for the interval. Unlike in the SPeAD-M86 model, this *scale height coefficient* is not necessarily a physical representation of the actual scale height. Deviation from the scale height tabulated by Wertz and Larson[13] was necessary to maintain the piece-wise formulation in Eq. (7) without requiring additional input or lookup variables. Tables 3 and 4 in the Appendix are the lookup tables for ρ_{max} and ρ_{min} respectively.

III.C. Calibration

The accuracy of any approximation model is dictated by the empirical data against which it is calibrated. Adhering to the design of the original SPeAD-M86 model, MSIS-86 atmospheric density data tabulated by Wertz and Larson[13] were used for the calibration. An MSIS model was selected for the calibration data set as it demonstrates slight improvements over the Jacchia models.[14] The scale height coefficient, H_i, and scale density, ρ_{s_i} required to compute ρ_{max} and ρ_{min} based on altitude were obtained by curve fitting to the published MSIS-86 density data.[13] The data are averaged across the Earth with a 30° step size in longitude and a 20° step size in latitude. Data corresponding to ρ_{max} were for a maximum solar flux $F_{10.7} = 189.0 \times 10^{-22}$ W·m^{-2}·Hz^{-1} while data for ρ_{min} were for a minimum solar flux $F_{10.7} = 65.8 \times 10^{-22}$ W·m^{-2}·Hz^{-1}.

To ensure the piece-wise exponential approach provided a continuous set of densities at all altitudes, it was essential to calibrate H_i and ρ_{s_i} precisely against the published datasets. Starting from Eq. (7), taking the natural logarithm, and isolating terms, we obtain

$$ln\left[\rho(z)\right] = \left[\frac{-1}{H_i}\right] z + ln\left[\rho_{s_i}\right] \tag{8}$$

which is in the form $y = mx + c$. H_i therefore represents the negative inverse of the slope between points on a density vs. altitude semi-log curve, while ρ_{s_i} represents the y-intercept. At altitudes above 1000 km, the density is set to zero. Columns 1 and 2 of Table 3 contain the interval data relevant to ρ_{max}, while columns 3 and 4 present the calibrated values of H_i and ρ_{s_i}. Table 4 presents the interval data for ρ_{min} in an identical manner.

IV. Validation Routines

Three techniques were utilized in order to validate the proposed model. First, in order to confirm that the SPeAD-M86 FX model correlated with published atmospheric datasets, a direct density vs. altitude comparison was undertaken. Next, the stability and accuracy of the model was verified in an orbit and attitude propagator implemented using the MATLAB-Simulink simulation environment. A 3U CubeSat in LEO with no active control system was considered for this study. The SPeAD-M86 FX and SPeAD-M86 models were evaluated against a NRLMSISE-00 model model. The initial classical orbital elements of the satellite with respect to Earth were defined as follows.

$$[a_0 \quad e_0 \quad i_0 \quad \Omega_0 \quad \omega_0 \quad \nu_0] = [6878 \text{ km} \quad 0.05 \quad 0.1^\circ \quad 270^\circ \quad 90^\circ \quad 0^\circ]$$

The elements correspond to a 156.1 km × 843.9 km orbit having a period of 94.6 minutes, with a low inclination of 0.1° to the equatorial plane of the Earth. Such an "atmosphere grazing" orbit could result from a failed circularization burn by the launch/deployment vehicle. Though unlikely for a CubeSat, it provides a scenario in which the atmospheric drag has a significant effect on the spacecraft near perigee. Furthermore, it allows the SPeAD-M86 FX model to be evaluated over a wide range of altitudes. The simulations for this orbit were conducted at 0.0, 2.0, 5.5, 7.0, and 10.0 years since solar minimum so as to fully assess the temporal accuracy of the model. Finally, in order to provide performance data for a more typical nanosatellite orbit, the same 3U CubeSat was simulated in a near-circular orbit with initial classical orbital elements

$$[a_0 \quad e_0 \quad i_0 \quad \Omega_0 \quad \omega_0 \quad \nu_0] = [6878 \text{ km} \quad 0.005 \quad 0.1^\circ \quad 270^\circ \quad 90^\circ \quad 0^\circ]$$

which correspond to a 465.6 km × 534.4 km orbit having a period of 94.6 minutes, with a low inclination of 0.1° to the equatorial plane of the Earth. For this simulation, a 1 second time step was utilized, in order to emulate a low computation propagator, as would be implemented on-board a CubeSat. The simulations for this near-circular orbit were conducted at 5.5, 7.0, and 10.0 years since solar minimum.

The time variation of the orbital elements using the SPeAD-M86 FX model was compared against the variation computed using the NRLMSISE-00 model available in Simulink. The NRLMSISE-00 model was selected as a baseline as it has been recommended by NASA to become the standard for use in satellite orbit prediction.[6,15] During validation of the original SPeaD-M86 model, a larger decrease in runtime was observed for high fidelity simulation environments.[7] Therefore, in order to highlight any computational advantages of the SPeAD-M86 FX model, simplified simulation environments, such as those utilizing lower-order gravity models and State Transition Matrix attitude propagation, were not considered. Though runtime reduction was found to be independent of time step during SPeAD-M86 validation, it was necessary to determine if this held true for the extended model. Given that the model applications are primarily for GN&C and short-term orbital prediction purposes, a 1-day simulation period was deemed sufficient for validations. The simulation environments and associated parameters are summarized in Table 1.

Parameter	Environment A	Environment B
Time step, Δt (sec)	0.1	1
Gravity model type	Spherical	Spherical
Order of gravity model	8	8
Attitude propagation	Quaternion EoM	Quaternion EoM
Attitude integrator	ode3	ode3

Table 1: Summary of Simulation Environment

Both environments included the effects of gravity gradient torque, atmospheric drag, and atmospheric torque, while utilizing the ode3 (Bogacki-Shampine) integrator for orbit propagation over a simulation time of 86,400 seconds. All simulations were run on a single logical thread of an Intel®Core™ i7 2700K 4.2 GHz processor with 16 GB available memory.

Geomagnetic index data, required as an input for the NRLMSISE-00 model, was taken from NOAA[16] for noon of May 1 1996, May 1 1998, December 1 2001, May 1 2003, and May 1 2006. These dates correspond to 0.0, 2.0, 5.5, 7.0, and 10.0 years from the start of Solar Cycle 23. Average solar flux index $F_{10.7a}$ and daily solar flux index $F_{10.7}$ data were obtained for the same dates as observed and derived from the GPS IONO model.[17] In addition, anomalous oxygen calculations were switched on for the NRLMSISE-00 model.

The orbital element error for the first five (a, e, i, Ω, ω) orbital elements was calculated as a percentage error using the NRLMSISE-00 data as the baseline. However, due to the cyclic nature of ν from 0 to 2π rad., such a quantification would not provide a clear representation of the actual error. Instead, the smallest difference in ν at each time step was calculated, and normalized against a full orbit (i.e. 2π rad) in a manner previously utilized by Kedare and Ulrich.[7] In addition to examining the accuracy and sensitivity of the SPeAD-M86 FX model, it was essential to quantify and compare the CPU run time against a NRLMSISE-00 baseline. The run times were obtained using the `tic - toc` functions in MATLAB, and averaged over 10 simulation runs for each environment.

V. Simulation Results

This section summarizes the results of the validation routines presented in Sec. IV.

V.A. Atmospheric Density

Figure 2 presents the density as computed by the SPeAD-M86 FX model at $t = 0.2, 1, 2, 3, 4, 5$ years alongside published density data from several atmospheric models. These temporal points correspond to instances spanning the increase in solar activity from its minimum to its maximum from $0 < t < 5.5$. During this timeframe, density at a given altitude is expected to increase with time. A reverse trend, with density decreasing at a given altitude, would be observed for the second half of the solar cycle, for $5.5 < t < 11$.

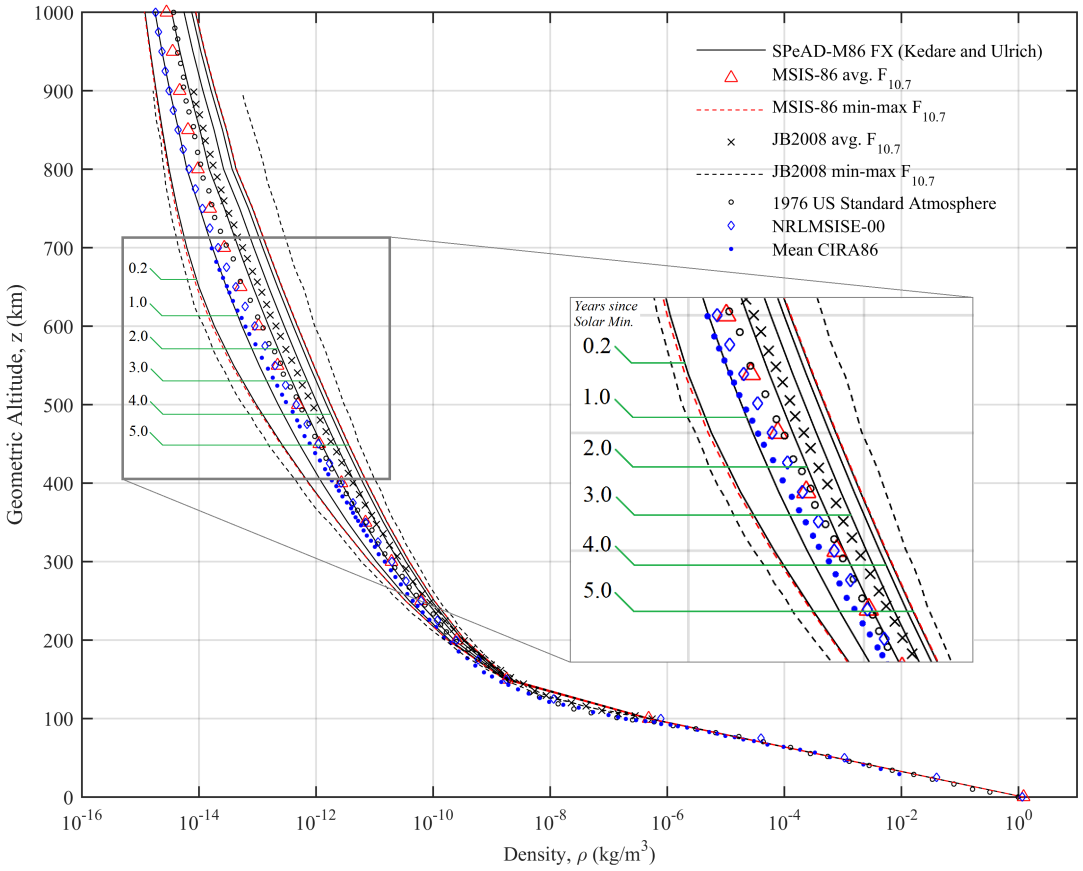

Figure 2. Density Comparison

In Fig. 2, the SPeAD-M86 FX data closely matches published empirical data from a number of models. At $t = 0.2$, corresponding to 2.5 months after the $F_{10.7}$ solar minimum, the density estimate provided by the model closely matches the MSIS-86 calibration data. As t is increased, the density curve shifts upwards towards the mean density data points. At $t = 2$, an even scatter of empirical data points about the SPeAD-M86 FX dataset is observed, indicating an overlap with mean solar activity. As t is further increased, the computed density approaches the MSIS-86 maximum density. Following the solar cycle peak at $t = 5.5$ years, the curve would begin to shift downward towards the minimum density (plots omitted for clarity). Between 100 km and 150 km, the SPeAD-M86 FX model demonstrates a small departure from published data, with the estimated density being greater than that suggested by the data. This discrepancy was previously observed in the SPeAD-M86 model,[7] and is a consequence of the model's piece-wise exponential nature.

CubeSats, however, typically operate at altitudes well above 150 km, and the departure from published data is not considered to diminish the applicability of the model.

V.B. Orbital Element Error: Environment A

This section presents the validation results for the eccentric orbit simulation within Environment A. The orbital elements errors were obtained as detailed in Sec. IV, and a comparison was made between the SPeAD-M86 FX and NRLMSISE-00 implementations, with the latter used as the baseline. Error data obtained from implementing the original SPeAD-M86 model was also included for comparison purposes. Figure 3 presents the orbital element error from implementing the SPeAD-M86 models and NRLMSISE-00 in Environment A for May 1 1996, the beginning of Solar Cycle 23.

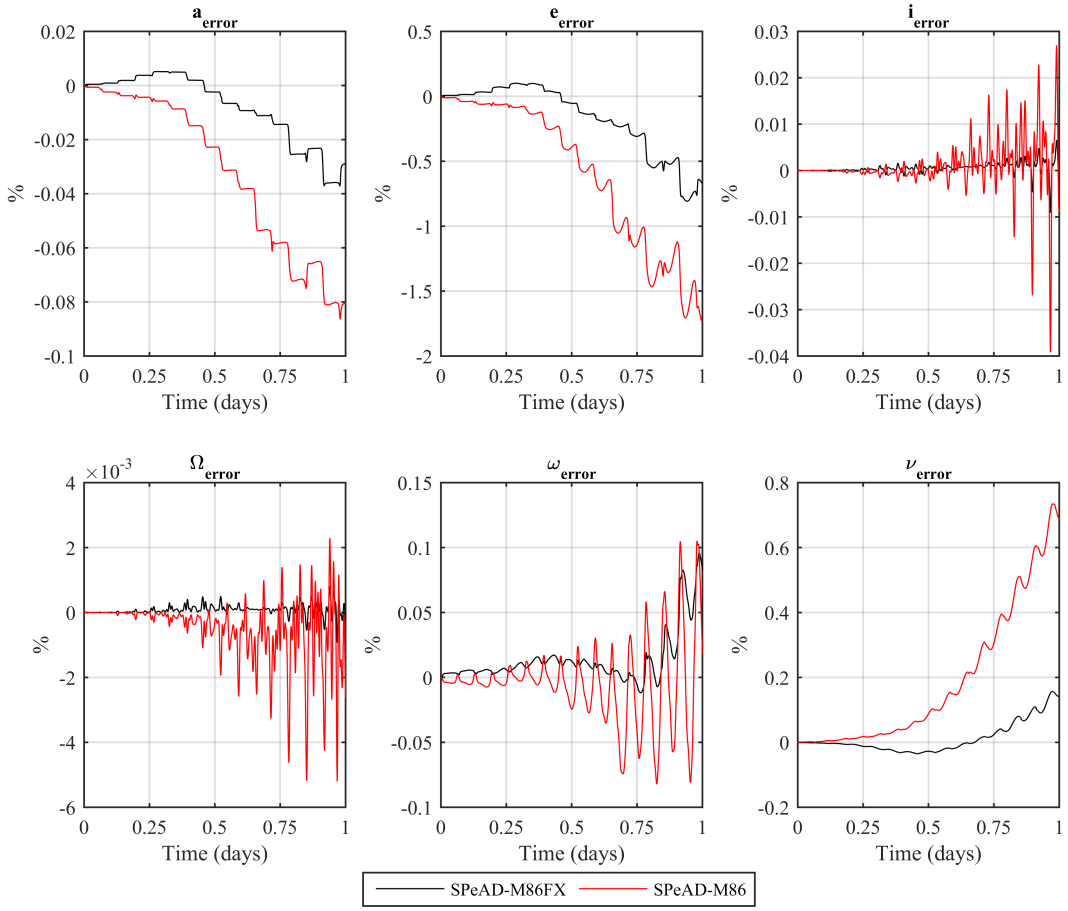

Figure 3. Environment A: Orbital element error for May 1 1996

It is evident that near the solar minimum, the SPeAD-M86 FX model outperforms SPeAD-M86 in orbit prediction accuracy. In particular, a_{error} and e_{error}, relating to the shape of the orbit, decrease significantly. For the duration of the simulation, the largest error for a and e remains under 0.04% and 1% respectively. Elements relating to the orientation of the orbit (i, Ω, ω) appear to closely follow the NRLMSISE-00 baseline. As with the SPeAD-M86 model, these errors increase in an oscillatory manner over time. However, the amplitude of these oscillations is greatly reduced. Finally, the location of the spacecraft in the orbit, ν, shows an error of approximately 0.15%. Figure 4 presents the orbital element error from implementing the SPeAD-M86 models and NRLMSISE-00 in Environment A for May 1 1998, 2 years into a typical solar cycle.

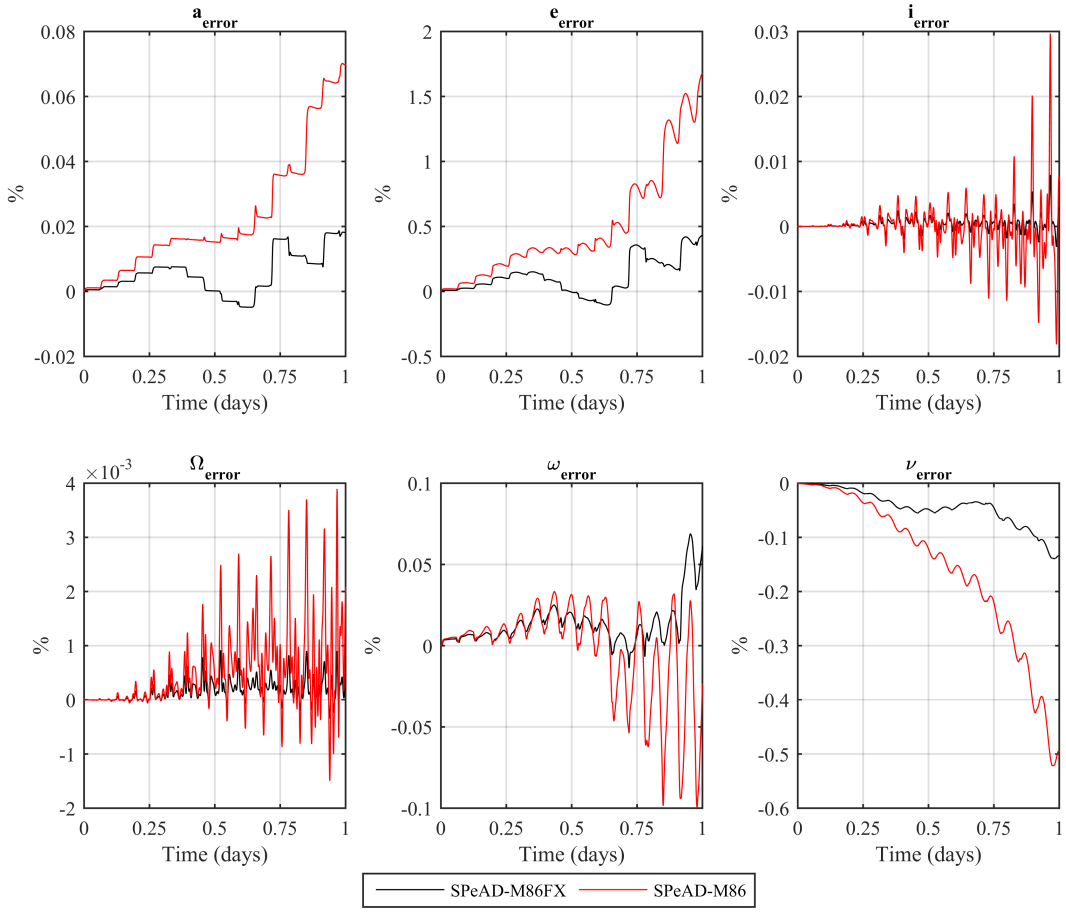

Figure 4. Environment A: Orbital element error for May 1 1998

Advancing past the solar minimum, the SPeAD-M86 FX model continues to demonstrate gains in accuracy compared to the SPeAD-M86 model. Errors in a and e are reduced by a factor of $\frac{2}{3}$ as a result of the SPeAD-M86 FX model accounting for the increase in ρ from rising solar activity. Errors in i, Ω, and ω indicate better consistency and smaller oscillation amplitudes over the duration of the simulation. Reductions in ν_{error} appear to be of similar magnitude as a_{error} and e_{error}. Figure 5 presents the orbital element error from implementing the SPeAD-M86 models and NRLMSISE-00 in Environment A for December 1 2001, 5.5 years into a typical solar cycle.

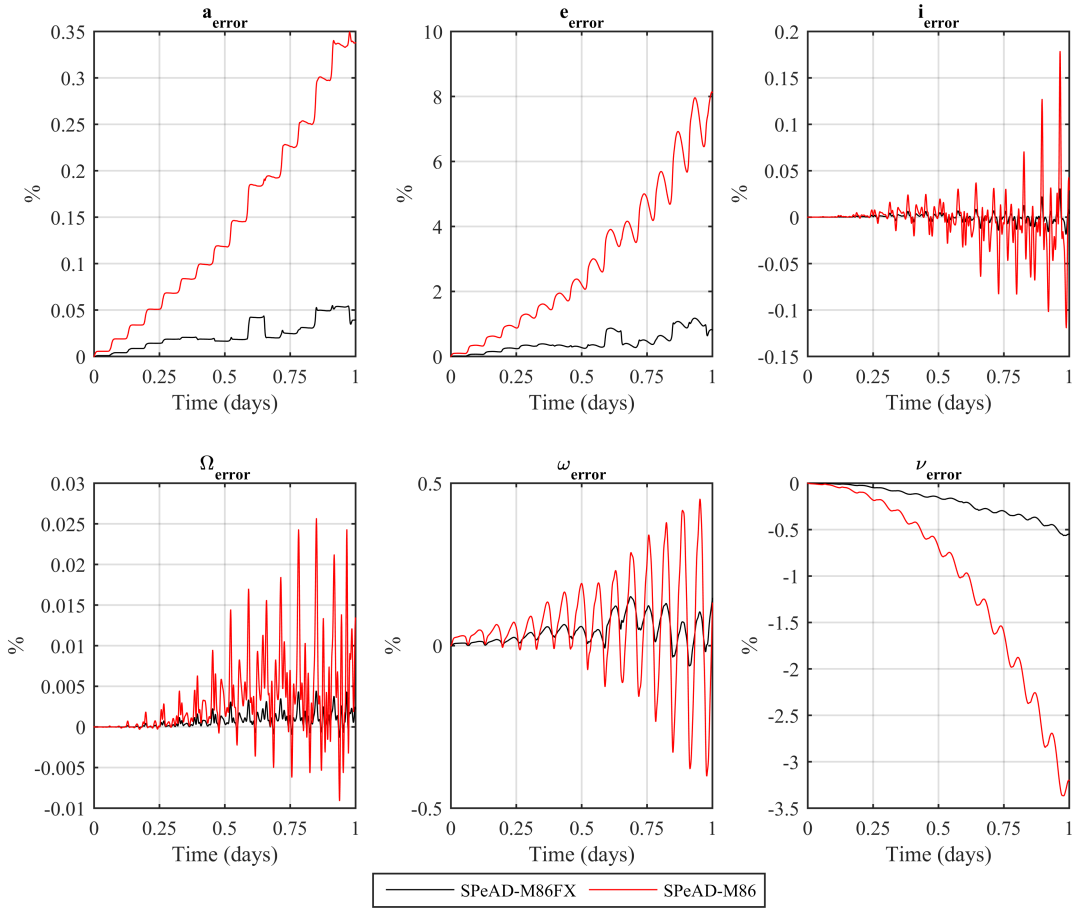

Figure 5. Environment A: Orbital element error for December 1 2001

Approaching the solar maximum, the SPeAD-M86 FX model shows significant gains in accuracy compared to the SPeAD-M86 model. Errors in a and e are reduced by a factor of $\frac{4}{5}$. Though error reductions in i, Ω, and ω are less pronounced, substantial declines in oscillation amplitudes are observed. The reduction in ν_{error} is again of comparable magnitude to a_{error} and e_{error}. Figure 6 presents the orbital element error from implementing the SPeAD-M86 models and NRLMSISE-00 in Environment A for May 1 2003, 7 years into a typical solar cycle.

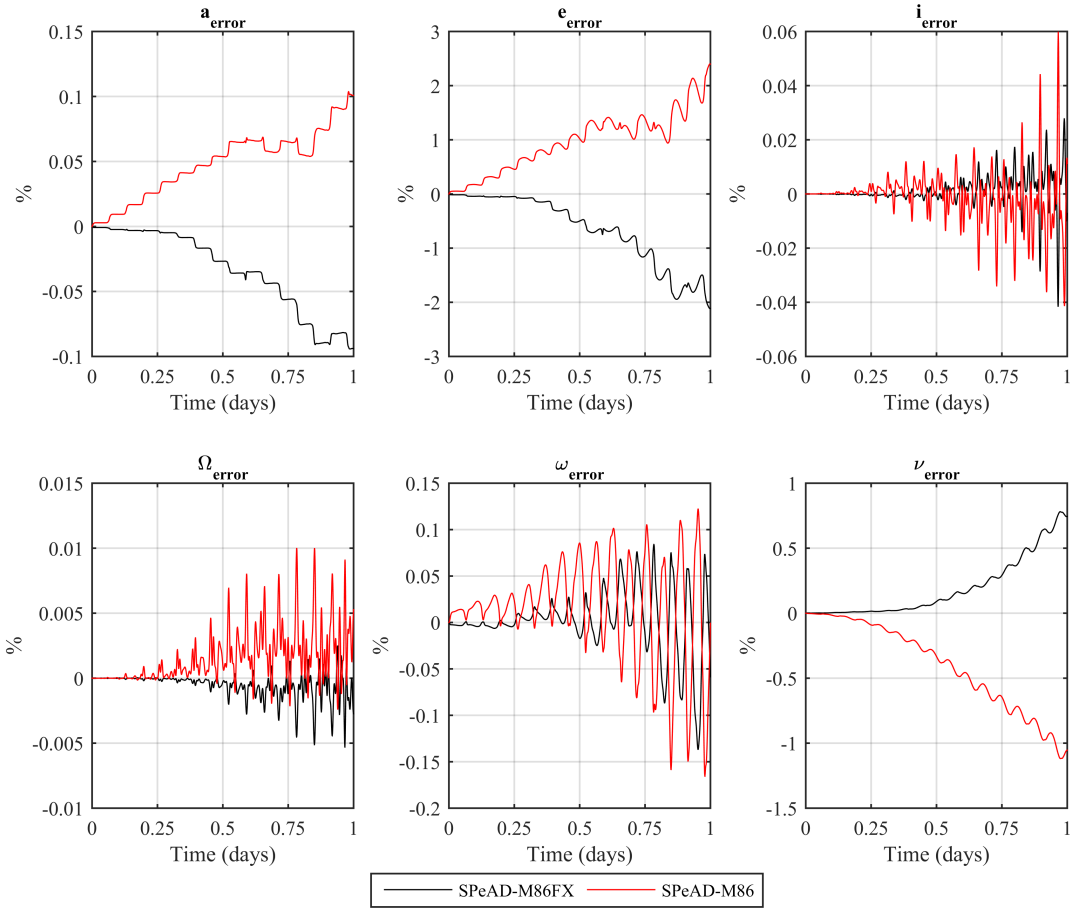

Figure 6. Environment A: Orbital element error for May 1 2003

Moving beyond the solar maximum, the orbital element error using the SPeAD-M86 FX model is similar to that obtained using SPeAD-M86. Errors for i, Ω, and ω demonstrate smaller amplitude oscillations. However, due to higher than average solar activity during cycles 21 and 22 (which contribute data towards the MSIS-86 model), the SPeAD-M86 FX model intermittently overpredicts density compared to NRLMSISE-00. This results in a small overprediction in orbital decay, leading to the corresponding errors in a, e, and ν. Figure 7 presents the orbital element error from implementing the SPeAD-M86 models and NRLMSISE-00 in Environment A for May 1 2006, 10 years into a typical solar cycle.

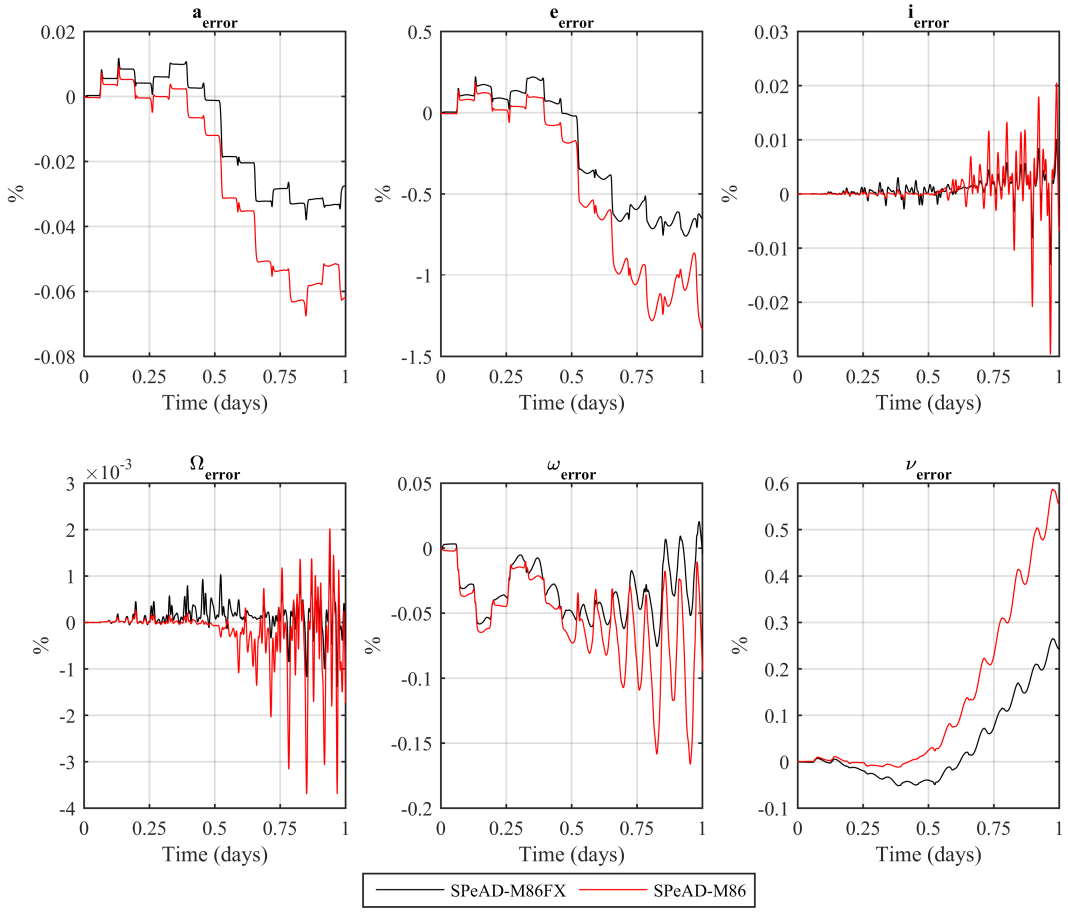

Figure 7. Environment A: Orbital element error for May 1 2006

Nearing the end of the solar cycle, the SPeAD-M86 FX model shows slight improvements over SPeAD-M86. For the first half of the simulation duration, errors for both SPeAD models are comparable. For the second half, the extended model demonstrates increased accuracy in orbit prediction, with error reductions of up to a factor of $\frac{1}{2}$.

V.C. Orbital Element Error: Environment B

This section discuses the validation results for the near-circular orbit simulation using Environment B. Figure 8 presents the orbital element error from implementing the SPeAD-M86 models and NRLMSISE-00 in Environment B for December 1 2001, 5.5 years into a typical solar cycle.

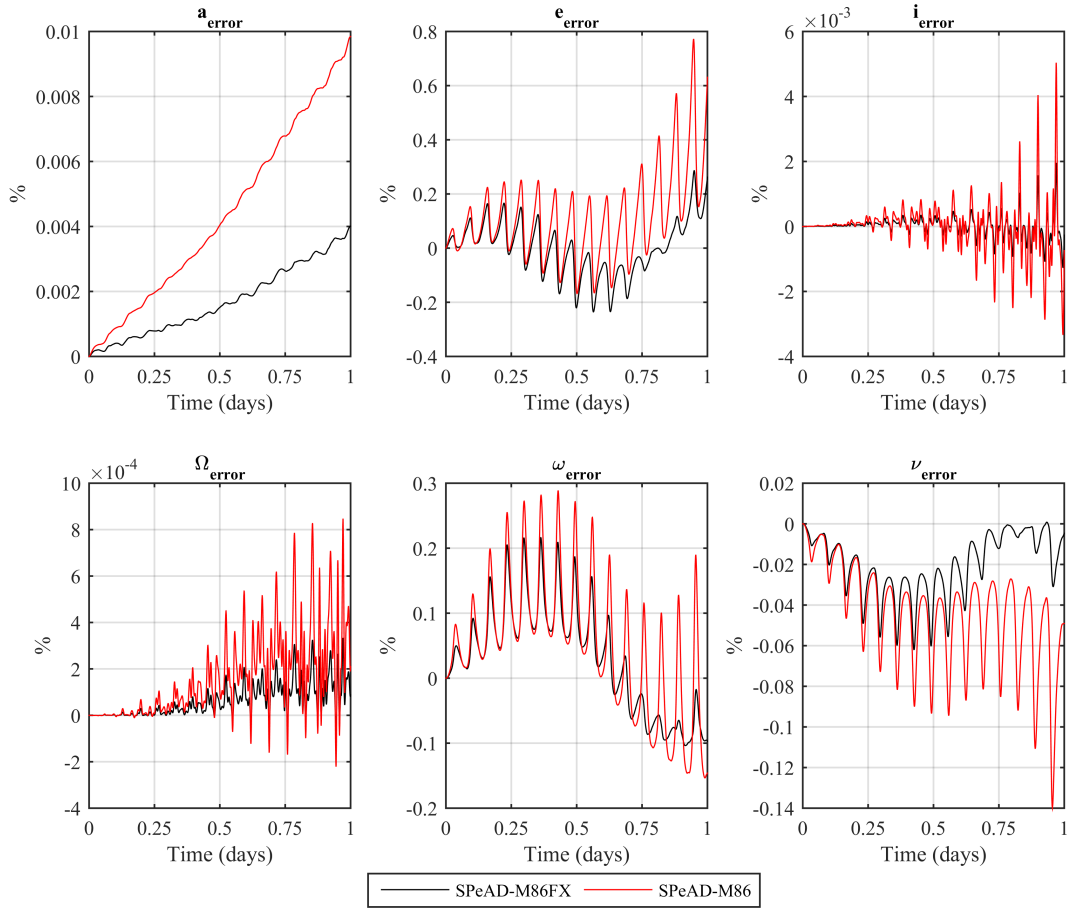

Figure 8. Environment B: Orbital element error for December 1 2001

Near solar maximum, the results indicate a reduction in orbital element errors compared to the SPeAD-M86 implementation. The largest orbital element error remains under 0.3% for the duration of the simulation, compared to 0.8% using SPeAD-M86. Orbital elements relating to the shape of the orbit (a, e) correlate well with the NRLMSISE-00 implementation, with the extended model further reducing error. The elements relating to the orientation of the orbit (i, Ω, ω) also closely follow the NRLMSISE-00 baseline. The error appears to increase in an oscillatory manner over time, particularly for i and Ω. Finally, the extended model reduces ν_{error} significantly. The inclusion of simplified $F_{10.7}$ effects provides increased accuracy due to the ability to capture secular density variations. Figure 9 presents the orbital element error from implementing the SPeAD-M86 models and NRLMSISE-00 in Environment B for May 1 2003, 7 years into a typical solar cycle.

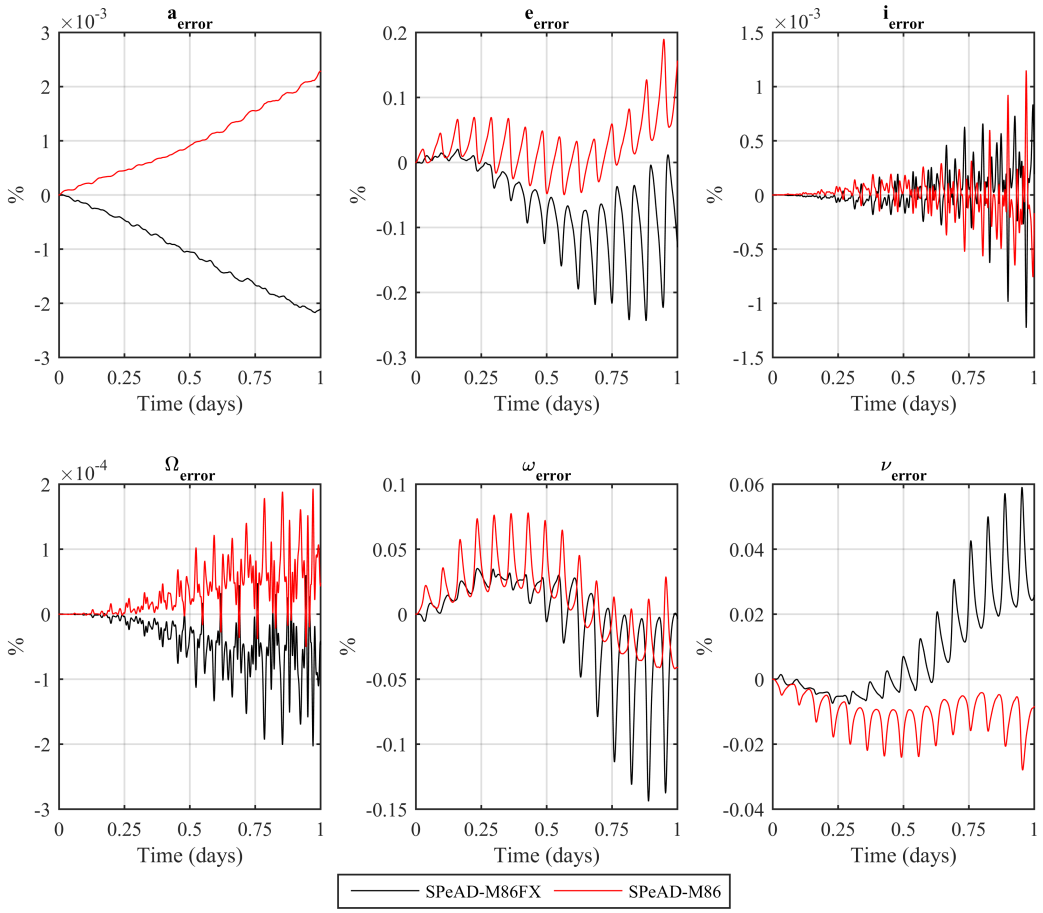

Figure 9. Environment B: Orbital element error for May 1 2003

Beyond the solar maximum, the orbital element error using the SPeAD-M86 FX model is similar to that obtained using SPeAD-M86. Errors for i, Ω, and ω demonstrate similar oscillations. However, as discussed earlier regarding Fig. 6 in Sec. V.B , due to higher than average solar activity during cycles 21 and 22 (which contribute data towards the MSIS-86 model), the SPeAD-M86 FX model may intermittently overpredict density compared to NRLMSISE-00. This results in a small overprediction in orbital decay, leading to the corresponding errors in a, e, and ν. Figure 10 presents the orbital element error from implementing the SPeAD-M86 models and NRLMSISE-00 in Environment B for May 1 2006, 10 years into a typical solar cycle.

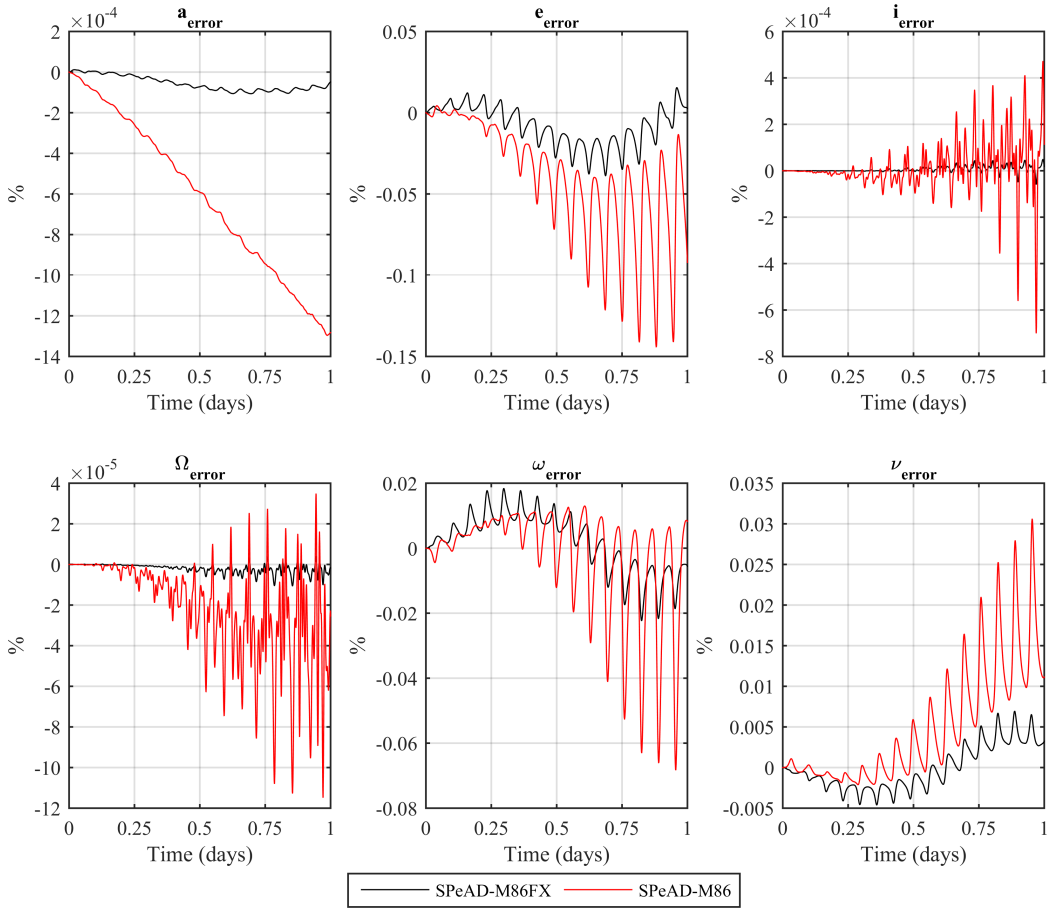

Figure 10. Environment B: Orbital element error for May 1 2006

Nearing the minimum in solar activity, the SPeAD-M86 FX model's ability to account for low solar activity leads to significant gains in orbit prediction accuracy. Errors in a and e, relating to orbit shape, are reduced substantially, while errors in i, Ω, and ω, relating to orbit orientation, show smaller oscillation amplitudes. ν_{error} is also reduced by a factor similar to e_{error}.

V.D. CPU Runtime

In addition to examining the accuracy and sensitivity of the SPeAD-M86 FX model at various points within the solar cycle, it was important to compare the CPU run time against the SPeAD-M86 model and the NRLMSISE-00 baseline. These results are summarized in Table 2.

Environment	Atmospheric Model	Average Run Time (sec)	Run Time Difference
A	NRLMSISE-00	201.2	–
	SPeAD-M86	160.8	↓ 20.1%
	SPeAD-M86 FX	169.3	↓ 15.9%
B	NRLMSISE-00	19.93	–
	SPeAD-M86	16.37	↓ 17.9%
	SPeAD-M86 FX	17.07	↓ 14.4%

Table 2: Simulation CPU Run Times

For both environments, the use of the SPeAD-M86 FX model result in a substantial decrease in run time over the NRLMSISE-00 model, ranging from 14.4% to 15.9%. The extended model does not appear to significantly increase computational overhead compared to SPeAD-M86, despite the inclusion of additional

look-up tables and trigonometric functions. Run-time reduction appears to be marginally dependent on the simulation time step, with larger improvements seen for a smaller time step.

VI. Conclusion

In this paper, a sinusoidal temporal correlation was incorporated into the SPeAD-M86 model to capture the effects of solar cycle $F_{10.7}$ variations on atmospheric density. Unlike existing atmospheric models which include $F_{10.7}$ effects, the SPeAD-M86 FX model only requires two variables: spacecraft position and the time since solar minimum. The computed density using the extended density model fits well with density data from previously published empirical models. Spacecraft orbit propagations agree closely with the NRLMSISE-00 baseline, and demonstrate improved accuracy compared to SPeAD-M86, hence establishing the stability and validity of the SPeAD-M86 FX model. Furthermore, the SPeAD-M86 FX model reduces CPU run time by 15% compared to NRLMSISE-00, making it suitable for use on board low-computational space platforms such as CubeSats.

Future improvements to this model could incorporate a Fourier series expansion in place of a simple sinusoidal formulation of the $F_{10.7}$ variation to better approximate the actual solar cycle. Accounting for geomagnetic activity, the diurnal bulge, and the thermal inertia of the atmosphere could further improve accuracy. Finally, on-orbit experimental drag observations would allow for better calibration and improvement of the model's long-term accuracy.

Appendix

Altitude Interval, km	MSIS-86 Base Density, kg/m^3	H_i (km)	ρ_{s_i}, kg/m^3
0 - 100	1.225	6.81	1.225
100 - 150	5.10E-07	9.06	3.19E-02
150 - 200	2.04E-09	28.46	3.97E-07
200 - 250	3.52E-10	41.66	4.28E-08
250 - 300	1.06E-10	50.78	1.46E-08
300 - 350	3.96E-11	57.51	7.30E-09
350 - 400	1.66E-11	63.46	4.12E-09
400 - 450	7.55E-12	67.77	2.76E-09
450 - 500	3.61E-12	71.85	1.90E-09
500 - 550	1.80E-12	75.10	1.40E-09
550 - 600	9.25E-13	78.44	1.03E-09
600 - 650	4.89E-13	81.11	7.98E-10
650 - 700	2.64E-13	85.39	5.34E-10
700 - 750	1.47E-13	88.78	3.90E-10
750 - 800	8.37E-14	77.48	1.34E-09
800 - 850	4.39E-14	131.33	1.94E-11
850 - 900	3.00E-14	110.74	6.47E-11
900 - 950	1.91E-14	122.52	2.96E-11
950 - 1000	1.27E-14	138.00	1.24E-11

Table 3: Altitude Interval Data for maximum solar activity, $F_{10.7} = 189.0 \times 10^{-22}$ W·m^{-2}·Hz^{-1}

Altitude Interval, km	MSIS-86 Base Density, kg/m^3	H_i (km)	ρ_{s_i}, kg/m^3
0 - 100	1.225	6.76	1.225
100 - 150	4.61E-07	8.88	3.60E-02
150 - 200	1.65E-09	22.45	1.31E-06
200 - 250	1.78E-10	29.94	1.42E-07
250 - 300	3.35E-11	35.50	3.84E-08
300 - 350	8.19E-12	39.91	1.51E-08
350 - 400	2.34E-12	43.02	7.98E-09
400 - 450	7.32E-13	46.02	4.36E-09
450 - 500	2.47E-13	49.42	2.23E-09
500 - 550	8.98E-14	55.20	7.71E-10
550 - 600	3.63E-14	64.90	1.74E-10
600 - 650	1.68E-14	82.14	2.50E-11
650 - 700	9.14E-15	107.48	3.87E-12
700 - 750	5.74E-15	137.49	9.33E-13
750 - 800	3.99E-15	167.45	3.52E-13
800 - 850	2.96E-15	191.56	1.93E-13
850 - 900	2.28E-15	211.52	1.27E-13
900 - 950	1.80E-15	224.07	9.99E-14
950 - 1000	1.44E-15	240.80	7.44E-14

Table 4: Altitude Interval Data for minumum solar activity, $F_{10.7} = 65.8 \times 10^{-22}$ W·m^{-2}·Hz^{-1}

References

[1]Tribble, A. C., *The Space Environment: Implications for Spacecraft Design*, Princeton University Press, Princeton, New Jersey, 2003.

[2]Walterscheid, R. L., "Solar Cycle Effects on the Upper Atmosphere: Implications for Satellite Drag," *Journal of Spacecraft and Rockets*, Vol. 26, No. 6, 1989, pp. 439–444.

[3]National Technical Information Service, *U.S. Standard Atmosphere*, Springfield, Virginia, 1976, Product Number: ADA-035-6000.

[4]Bowman, B. R., Tobiska, W. K, Marcos, F., and Huang, C., "The Thermospheric Density Model JB2008 using New EUV Solar and Geomagnetic Indices," *37th COSPAR Scientific Assembly*, Annapolis, MD, July 13–20 2008, p. 367, Symposium C, session 42 (oral). Paper number: C42-0004-08.

[5]Jacchia, L. G., "Revised Static Models for the Thermosphere and Exosphere with Empirical Temperature Profiles," *SAO Special Report No. 332*, Smithsonian Institution Astrophysical Observatory, Cambridge, MA, 1971.

[6]Picone, J. M., Hedin, A. E., Drob, D. P. and Aikin, A. C., "NRLMSISE-00 Empirical Model of the Atmosphere: Statistical Comparisons and Scientific Issues," *Journal of Geophysical Research*, Vol. 107, No. A12, 2002.

[7]Kedare, S. S., and Ulrich, S., "Design and Evaluation of a Semi-Empirical Piece-wise Exponential Atmospheric Density Model for CubeSat Applications," *AIAA Modeling and Simulation Technologies Meeting*, Kissimmee, FL, 5-9 January 2015.

[8]Simon, R., *Catalog of Earth Satellite Orbits: Achieving and Maintaining Orbit*, 2009 (accessed November 28, 2015), http://earthobservatory.nasa.gov/Features/OrbitsCatalog/.

[9]Visentine, J. T. (ed.), "Atomic Oxygen Effects Measurements for Shuttle Missions STS-8 and 41-G," *NASA TM-100459*, Vol. I-III, Sept. 1988.

[10]Hathway, D. H., "The Solar Cycle," *Living Reviews in Solar Physics*, Vol. 7, 1994, pp. 1, URL (cited on 24 May, 2015): http://www.livingreviews.org/lrsp-2010-1.

[11]Tapping, K. F. and Charrois, D. P., "Limits to the accuracy of the 10.7 cm flux," *Solar Physics*, Vol. 150, No. 1-2, 1994, pp. 305–315.

[12]Emmert, J. T., Lean, J. L., and Picone, J. M., "Record-low thermospheric density during the 2008 solar minimum," *Geophysical Research Letters*, Vol. 37, 2010, L12102.

[13]Wertz, J. R. and Larson, W. J., *Space Mission Analysis and Design, 2nd ed.*, Microcosm and Springer, Hawthorne, CA, 2008.

[14]Akins, A., Healy, L., Coffey, S., and Picone, M. , "Comparison of MSIS and Jacchia Atmospheric Density Models for Orbit Determination and Propagation," *13th AAS/AIAA Space Flight Mechanics Meeting*, Ponce, Puerto Rico, February 9-13 2003, Paper AAS 03-165.

[15]Picone, J.M., Drob, D.P., Meier, R.R., and Hedin, A.E., "NRLMSISE-00: A New Empirical Model of the Atmosphere," *NRL Review*, 2003, http://www.nrl.navy.mil/research/nrl-review/2003/atmospheric-science/picone/.

[16]NOAA, *NOAA National Geophysical Data Center FTP Site*, 2014 (accessed May 26, 2014), ftp://ftp.ngdc.noaa.gov/STP/GEOMAGNETIC_DATA/INDICES/KP_AP/2007.

[17]NorthWest Research Associates, Inc. Space Weather Services, *10.7 cm Solar Radio Flux*, 2014 (accessed May 15, 2014), http://www.nwra.com/spawx/f10.html.